Evaporation rates from square capillaries limited by corner flow viscous losses

Frouke Hoogland, May 2012

A master thesis for the master program Environmental Hydrogeology at the Department of Earth Sciences, University of Utrecht, The Netherlands

This research was conducted at the Soil and Terrestrial Environmental Physics (STEP) group, Department of Environmental System Science, ETH Zürich, Switzerland under supervision of prof. Dani Or (ETH), dr. Peter Lehmann (ETH) and prof.dr. ir. Majid Hassanizadeh (UU)

Abstract

Evaporation is an important process in water exchange between soil and atmosphere as well as applications in industry. Predictions of drying rates from porous media are very difficult due to its highly non-linear behavior with typically high and fairly constant drying rates in the beginning followed by a drop to low rates. The high drying rates at the first stage of drying are attributed to the presence of liquid patches retained in corners of the partially air filled pore space that are interconnected to form conductive pathways. Under increasingly dryer circumstances these liquid connections break leading to the diffusion dominated low drying rates of the second stage. The maximum extent of this corner flow region that determines the duration of the first stage is controlled by capillary forces opposed by gravity and viscous losses. To quantify these mechanisms, evaporation is studied from a single glass capillary with square cross section. Such geometry shows similar drying curve characteristics as macro-scale porous media with high rates as long as thick capillary sustained corner films extent between the receding meniscus and capillary surface. Increased flow resistance and gravity force as drying proceeds lead to film break-up at certain characteristic meniscus depth L_C. L_C was studied experimentally for drying of liquids ethanol and water from different capillary sizes under a range of evaporation rates and capillary inclination

angles. This way the forces determining the extent of the corner films were changed systematically. Break-up of films as well as evolution of main meniscus depth were monitored to deduce L_C and drying rates. For ethanol initial evaporation rates were in the order of 1000 mm/day and dropped abruptly when the corner films broke up. Increasing the evaporation rate led to a shortening of the films, whereas with decreasing gravity component the films became significantly longer. Maximum corner film extent for water was much shorter and mainly limited by corner geometry due to its high contact angle of 30°. Model predictions on L_C based on force balance and corner flow equations gave good results that were in accordance with the experimental data. The roundedness of the capillary corners had a large influence on maximum film length by limiting the curvature of the liquid interface at the capillary surface. This roundedness represents a critical pore size in real porous media that determines the maximum extent of the corner film region.

1. Introduction

An understanding of the drying process from porous media is important for a number of different fields. Evaporation determines the exchange of water between soil and atmosphere which makes it an important parameter for determining water availability for plants and microorganisms. Furthermore drying processes are important in various industrial applications including food processing and preservation, and for example the drying of ceramics and paper [1].

During evaporation pores become increasingly invaded by air replacing the liquid that vaporizes into the gas phase and is transported outside of the medium into the atmosphere. The drying front can be defined as the interface below which all pores are saturated with liquid, and above which pores are partially invaded by air. As drying proceeds this front recedes inside the medium. The region above the drying front becomes increasingly dryer as the front moves down, however liquid patches are retained in the pore corners due to capillary forces. As drying proceeds these liquid patches become smaller and thinner. The distribution of this residual liquid above the drying front is highly dependent on the internal structure of the porous medium and has significant influence on its drying

curve. Therefore drying rates from real porous media are difficult to predict requiring extensive knowledge on the internal medium properties.

1.1 Drying stages

In numerous studies on evaporation from porous media a distinction is made between two drying stages characterized by different drying rates. During the first stage rates are high and rather constant which is attributed to a film region extending between drying front and the surface. In this film region liquid can be transported by advection through the capillary retained liquid in corners of the pore space. During this first stage the liquid transport inside the medium can be high enough to sustain the evaporative demand at the surface. Therefore drying rates are only limited by the mass exchange between medium surface and the air boundary layer above. In the second stage drying rates drop because the film region no longer extents up to the surface leading to a transition from advection dominated to diffusion dominated transport where diffusion is the much slower process

The first stage was defined as a constant rate period (CRP) by Scherer [2] because in this stage the drying rate per area remains constant and close to the potential evaporation rate that would be found at a free evaporating surface. In a review on existing theories on evaporation Van Brakel [3] noted however that in numerous experimental studies it is better to speak of a pseudo constant rate period since often drying rates in this stage are continuously dropping as water content at the surface decreases. Suzuki and Maeda [4] solved the differential equations for liquid evaporation from a discontinuous surface that consists of dry and wet patches, to a viscous boundary layer above. Their results show that potential drying rates depend on the thickness of the boundary layer where evaporation rate increases for thinner boundary layer due to an enhanced gradient in vapor concentration. Their results also show that drying rates from increasingly dry surfaces can be constant as long as the typical width of the wet patches at the surface is much smaller than the thickness of the viscous boundary layer. Experimental studies can show both cases where Lehmann et al. [1] found a stage 1 consisting of constant drying rates for low evaporative demand, but once

76 the initial drying rate exceeded a value around 4 mm/d the first stage showed continuously
77 decreasing drying rates. Even though such a pattern does not correspond to Scherer's description of
78 a CRP they could argue that this drop in drying rates was not due to limitations by low hydraulic
79 conductivity inside the medium but should be explained by limitations in the mass exchange
80 between the partially dry medium surface and the viscous boundary layer above. Thus during stage 1
81 of evaporation both constant drying rates as well as decreasing drying rates can be observed.
82 However for both cases the first drying stage is characterized by the fact that the transport inside the
83 medium is not limiting the observed drying rates.

84 When advectional transport inside the medium can no longer sustain demand at the surface, drying
85 rates become diffusion dominated and can be accurately described by Fick's law of diffusion as
86 shown by Shokri et al. [5]. In this stage diffusion takes place from a secondary evaporation front
87 above the drying front where the two are interconnected by liquid pathways. The secondary
88 evaporation plane during this stage is where phase change from liquid to vapor takes place as well as
89 salt depositions. Increasing diffusional pathways as drying proceeds lead to a continuous drop in
90 drying rates in the second stage of drying [5].

91 The two drying stages and their liquid distribution above the drying front in a porous medium are
92 illustrated by figure 1.

93

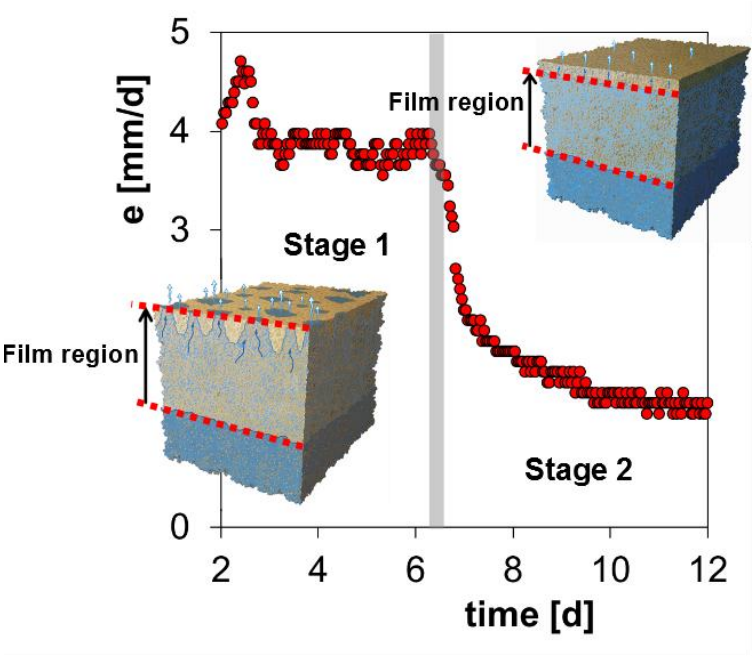

Figure 1: Measured evaporation rates from sand of grain sizes 0.3-0.9 mm as stated in Lehmann et al. [1].*During first stage of evaporation drying rate e is constant due to continuous liquid connections that extent between drying front and surface (as shown in the conceptual figure insets). Constant rates are followed by the low and decreasing drying rates of diffusion dominated stage 2. During this stage liquid has to evaporate from a secondary drying front (evaporation plane) and diffuse towards the surface. The duration of stage 1 is dependent on the maximum extent of the 'film region' where liquid connections exist due to capillary retained liquid patches.*

1.2 Film region

The high mass flow inside the medium during stage 1 is attributed by Yiotis et al. [6] to the presence of a film region between drying front and the medium surface from which mass exchange with the boundary layer takes place. In this film region continuous connections between liquid patches are present that are retained by capillarity. These liquid connections form flow paths leading to advection dominated transport and thus relatively high evaporation rates. Yiotis et al. [7] make a distinction between 'thick films' that consist of capillary retained liquid in crevices of the pore space and as pendular rings around the contact points between grains, and 'thin films' that are adsorbed to the pore walls. The latter are much thinner and thus have higher resistances to flow as quantified by

111 Tuller and Or [8] where they derived viscous resistances for both film types and different pore
112 geometries. Shokri et al. [5] used X-ray tomography on a sand filled column to image this film region
113 experimentally and found that the retained liquid above the drying front indeed formed a continuous
114 network.

115 **1.3 Characteristic length**

116 As long as the film region extents up to the surface drying rates are in advection dominated stage 1.
117 This means that the maximum film region extent controls the duration of this stage and as soon as it
118 retreats inside the medium the transition to diffusion controlled stage 2 takes place. Lehmann et al.
119 [1] define a characteristic depth of the front, L_C, at which capillary flow paths between front and
120 surface disconnect marking the end of stage 1. This front depth follows from the balance between
121 capillary force sustaining the film region, opposed by gravity and viscous losses. The capillary driving
122 force is generated by the pressure difference between liquid filled small pores at the surface and
123 larger pores at the drying front [1]. This generates a 'capillary pumping' mechanism as defined by
124 Yiotis et al. [9] leading to capillary driven flow to the small pores at the surface. Under hydrostatic
125 conditions the absolute pressure head increases linearly with distance from the drying front until it
126 reaches a critical head value h_{min} at the surface at which the film region becomes disconnected. In
127 this hydrostatic case the difference between air entry value at the front and h_{min} at the surface
128 equals the length at which the films will break-up and can be called the gravity length L_G [1] because
129 in such case only gravity is opposing the capillary force. In the case of evaporation, liquid flow occurs
130 through the film region leading to viscous losses that use part of the capillary pressure difference
131 which leads to earlier film break-up. When there is no gravity opposing flow, which is the case for a
132 horizontal capillary configuration, the entire capillary driving force can be used to overcome the flow
133 resistance. The resulting maximum film length can be defined as the viscous length L_V. When both
134 gravity and viscous losses are of importance the maximum front depth L_C follows from a combination
135 of the two. For coarse media viscous losses are of small importance and L_V is in general much larger
136 than L_G. For finer textured media flow resistance increases and L_C is determined by both gravity and

viscous losses. L_C can be in the range of several hundred mm for typical soil classes and evaporation rates as shown by Lehmann et al. [1].

1.4 Evaporation from angular pores

It is difficult to quantify the viscous losses in real porous media because they are dependent on the hydraulic conductivity of the medium. This varies with liquid content and depends on the internal structure of the medium. To gain more insight into the dynamics and extent of the film region the drying process from the simple geometry of a single capillary with square cross section can be studied. Drying from this simple geometry shows very similar dynamics as drying from real porous media. This has everything to do with the fact that in angular capillaries liquid volumes are retained in its corners by capillarity. These liquid volumes will be defined from here on as corner films. They provide a pathway for liquid to flow to the surface while the main meniscus is moving down as a result of liquid evaporation. This leads to significantly faster drying than if the films would not be present. Laurindo and Prat [10]did pore network simulations as well as experiments on a 2 dimensional micro network of interconnected ducts with square cross section. They recognized significant deviations of simulated and observed drying curves which they attributed to the presence of film flow in the experiments that the model did not take into account. Prat [11] extended this simulated pore network model to include corner film flow by simulating three different types of angular cross sections. The model including the corner flows could simulate the drying curves as observed in the experiments much more adequate. Chauvet et al. [12] did an experimental study on evaporation of heptane and 2-propanol from square capillaries and showed that ¨*evaporation in a square tube is much faster and dramatically different* (to that from a circular capillary) *owing to the effect of corner films*¨ [12]. Note that a circular capillary does not retain liquid above the main meniscus which results in drying rates that are immediately diffusion dominated from the beginning of evaporation. Chauvet et al. [12] recognized three different stages in the drying curves from the square capillary that are similar to the ones observed from drying in real porous media. A first period in which evaporation rate was constant and controlled by external demand, followed by a

transitional period in which drying rates show a significant drop and a last period where evaporation takes place from inside the medium/capillary. They state that the drop in drying rates can be directly linked to film detachment where films in the experiments in general detach slightly after the drying rates start to drop. Before film break-up the corner films extent between receding main meniscus and the surface which makes liquid flow possible inside the capillary. Due to this relatively fast transport mechanism drying rates in this stage are not limited by internal conditions of the capillary but by the external demand at the surface. As soon as the corner films break-up from the surface the phase change from liquid to vapor takes place from inside the capillary, and diffusion becomes the main transport mechanism as in stage 2. This indicates that drying from the square capillary is very similar to drying from real porous media by showing the same drying curve characteristics and underlying mechanics. It can thus be used as a conceptual model for evaporation, where corner films serve as an analogue for the film region while the main meniscus represents the drying front.

Just as the characteristic length of the film region as defined by Lehmann et al. [1] corner films have a maximum extent at which they will break-up from the surface. We define a characteristic meniscus depth L_C where corner film break-up occurs as a result of increased viscous losses and gravity force due to longer and thinner films as the meniscus moves down. L_C of the corner films is expected to be highly dependent on the viscous flow resistance since film cross sections are small. Thus we can use this concept to study the effects of both gravity and viscous losses on maximum film region extent.

The flow resistance in the corner films are mainly determined by the liquid distribution and flow rates. Numerous studies have already described the liquid distribution in an angular pore occupied by liquid and gas phase by relating the liquid/gas interfacial curvature to matric potential. Mason and Morrow [13] describe the liquid distribution in triangular tubes with different aspect ratio, for both drainage and imbibition, which show significant differences and thus hysteresis for both processes. Tuller et al. [14] focus on the respective contributions of adsorbing and capillary forces to liquid distribution in angular pores that are occupied by two phases. This led to analytical solutions for saturation as well as interfacial area as a function of matric potential and pore geometry. From the

189 liquid distribution the next step is to quantify flow through the corner films. Tuller and Or [8] study
190 flow through adsorbed thin films in slits and along the pore walls, as well as through thick films in the
191 corners held by capillary forces. Taking into account resistance to flow they derive analytical
192 solutions for average flow velocities and by upscaling relate this to the medium hydraulic
193 conductivity, saturation and interfacial area as a function of matric potential [15]. Dong and Chatzis
194 [16]did experiments as well as theoretical predictions on imbibition of 5 different liquids in a
195 horizontal square capillary to see effects of liquid properties on imbibition rates. Rates decreased
196 with increasing liquid contact angle due to smaller liquid filled cross sectional area as well as with
197 smaller tube sizes.

198 Corner geometry is of great influence on average flow rates. As stated by Chauvet et al. [17] a slightly
199 rounded corner has large implications on maximum film extent which is for a large part due to the
200 fact that it influences the resistance to flow. In a rounded corner the ratio of wetted perimeter to
201 liquid filled cross sectional area is increasing with thinning of the film leading to nonlinear increase in
202 flow resistance. Rounded corner effects as represented in a resistivity factor were assessed
203 numerically by Ransohoff and Radke [18], analytically and numerically by Chen et al. [19] and by
204 deriving analytical approximations by Zhou et al. [20].

205 Chauvet et al. [17] also studied L_C by experiments with two perfectly wetting liquids and model
206 development. We extent this further by also studying the drying dynamics of liquid with nonzero
207 contact angle (water) as well as film break-up under different capillary orientations. The focus is on
208 the effect and importance of viscous losses on L_C by varying evaporative demand and thus corner
209 flow and flow resistance. This was done by experiments on ethanol and water evaporation from two
210 different sizes of capillaries and by development of a corner flow model. We propose a simple
211 modeling strategy to predict L_C from capillary geometry, liquid properties as well as evaporative
212 demand.

213 **1.5 Objective**

The objective of this study is to quantify the mechanisms determining the maximum extent of the corner film region and the resulting drying stages using the simple model of a single square capillary. The study consists of an experimental part and a modeling part. In the experimental part the drying of liquids water and ethanol are studied from a single glass capillary with square cross section. Different capillary sizes are used. Furthermore different evaporation rates are applied to study the influence of viscous losses on the extent of the corner films. Also the capillary is put under different inclination angles of 0, 30 and 90° to vary the gravity component that opposes flow. In this way the influence of these forces on maximum film extent can be quantified. For the modeling part the maximum film length is determined as a function of initial evaporation rate based on corner flow equations and force balance.

The thesis is organized as follows: Section 2 describes the theoretical considerations determining liquid distribution and flow velocities of the corner films. Also the modeling approach is explained here with its underlying assumptions. Section 3 explains the experimental setup and methods after which the results of experiments and model are shown in Section 4. Section 5 gives a discussion on these results, followed by summary and conclusions in section 6.

2. Theoretical considerations

2.1 Capillarity and pore geometry

A schematic representation of a square shaped capillary is shown in figure 2. It shows the main meniscus at a certain depth defined as z_m, and the liquid corner films above both in a schematic representation as well as a real experimental image of the corner films. Capillary width is defined as d and depth z goes from zero at the surface to increasingly positive in the downward direction. In figure 3.a a cross section of a capillary corner is shown at a certain height above the main meniscus, showing the liquid retained in the corner with its radius of curvature r of the gas/liquid interface, as well as the corner geometry of a slightly rounded corner. The glass capillaries used in our experiments typically do not have perfectly sharp corners but instead have a certain radius of curvature r_0. Therefore in all following theoretical considerations this corner radius is taken into account which, as was shown by Chauvet et al. [17], is a very important parameter determining film break-up.

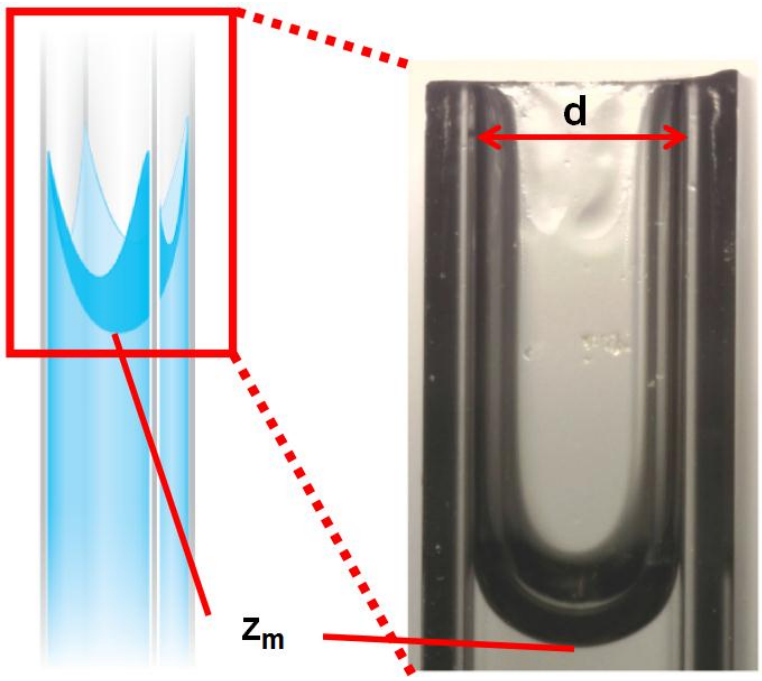

Figure 2: Schematic representation of a single square capillary on the left showing the liquid corner films as well as main meniscus position z_m. Right shows an experimental high magnified image of one

capillary wall with width d=1.0 mm, and two adjacent corner films. Note that the films become thinner towards the surface.

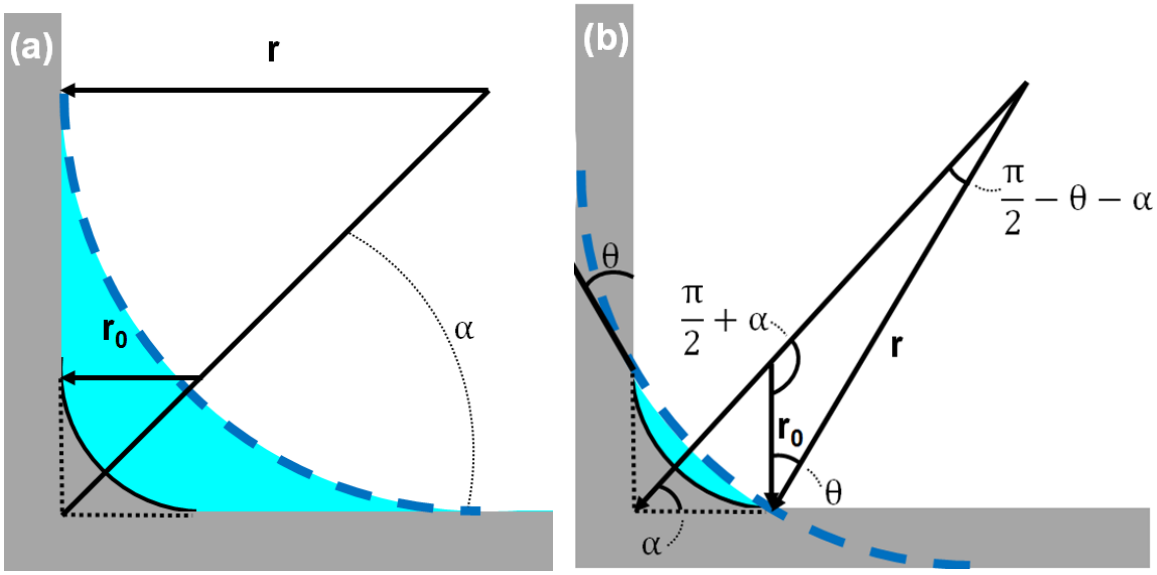

Figure 3: (a) shows a schematic representation of a capillary corner (half angle α) with corner radius r_0 and liquid distribution at a gas/liquid interfacial radius r. (b) shows a schematic representation of the same corner, with the minimum possible liquid radius r with contact angle ϑ for which liquid can still be retained in the corner by capillary forces.

Due to capillary forces liquid in a small tube rises up to a certain height above a zero pressure level depending on surface tension σ and degree of wetting (contact angle θ) of the liquid and on capillary geometry. In angular tubes capillary forces also lead to liquid retention in its corners above the main meniscus which is not the case in cylindrical capillaries. The curvature r of the corner changes with height above the main meniscus depending on pressure head h. The relationship between h and r is given by the Young Laplace equation:

$$\frac{\sigma}{r} = -\rho g h \qquad (1)$$

Where σ and ρ are respectively surface tension and density of the liquid and g is the gravitational acceleration. In the stated form of the Young Laplace equation only one direction of curvature is considered. This is reasonable along the major part of the liquid films. However from experimental

high magnified images of the films it can be seen that the z component of curvature does become important close to the top of the capillary. Chauvet et al. [17] observed this as well in their experimental results. In the same line of argument as they do we say that the distance over which this second direction of curvature is significant is of the order of one capillary width d, which is in general much smaller than the total film length. Thus it can be expected that taking curvature in the z direction into account will not have a significant effect and equation 1 can be used to give a direct relationship between h and resulting r in the cross-sectional plane.

During the process of evaporation liquid goes into the vapor phase due to a gradient in vapor concentration which leads to diffusional transport. The volume of the evaporated liquid is being replaced by the gas phase which makes the main meniscus retreat into the capillary. However in order to have gas invasion the air entry value of the capillary must be exceeded at the surface leading to a sudden jump from complete saturation to liquid retained only in the corners with a certain radius of curvature. The occurrence of this jump is often described as a pore snap off mechanism [8] [21]. The liquid distribution and pore snap-off mechanisms under a range of matric head values differ for different capillary geometries and for the different processes of drainage and imbibition. Tuller et al. [14] derived relationships for liquid distribution and hydraulic properties as a function of matric head and pore geometry defined with the corner half angle α. Since this paper only focuses on square geometries, derivations will only be given for α equal to $\pi/4$.

The value of h at which the capillary becomes air invaded is equal to the liquid rise of the main meniscus under equilibrium conditions and can be found by the Princen model [22]. It can be compared to the air entry value of real porous media and we define it as the snap off value for drainage h_d. The liquid rise results from the balance between capillary and gravity force where the capillary force along the liquid/solid contact line for a square capillary is given by:

$$F = 4\, d\, \sigma \cos\theta \qquad (2)$$

Where θ is the contact angle of the liquid with the solid capillary wall. The capillary force is balanced by the weight of the liquid below the main meniscus and the weight of liquid films above. The total weight can then be written as:

$$W = \rho g h_d \, d^2 + 4\rho g \int_{h_d}^{\infty} \left(1 - \frac{\pi}{4}\right) * r(z)^2 dz \quad (3)$$

r(z) follows from the hydrostatic case of equation 1 where h can be substituted by z. Solving for F equal to W and defining $\gamma = \frac{\sigma}{\rho g}$ gives the equilibrium height h_d of the main meniscus:

$$h_d = \frac{2\gamma \cos\theta + \gamma\sqrt{\pi - 2 + 2\cos 2\theta}}{d} \quad (4)$$

h_d can be linked to the snap off radius of curvature r_d that defines liquid distribution at the main meniscus by equation 1.

As said before the capillaries used in the experiments have a certain radius of curvature r_0 instead of sharp corners which has a large effect on L_c. Rounded corners provide a restriction on the minimum radius of curvature r of the liquid at which liquid can still be retained in the corners. To describe effects of a rounded corner we first define the degree of roundedness Ro:

$$Ro = \frac{r_0}{r(h)} \quad (5)$$

Chauvet et al. [17] as well as Zhou et al. [20] use the same definition of roundedness. The definition used by Ransohoff and Radke [18] is the same if a contact angle of 0 is assumed between the circle describing the rounded corner and the capillary wall. Chauvet et al. [17]studied the effect of rounded corners on maximum film extent by use of experiments with different capillaries having different corner radii. They found that the degree of roundedness of the corner is the most important parameter that influences maximum extent of the corner films by restricting liquid radius r at the capillary surface. For a perfectly wetting liquid (θ=0) once the curvature of the corner film r equals r_0,which corresponds to a roundedness Ro of 1, capillary forces can no longer retain the liquid and the film breaks up.

Chauvet et al. [17] only focus on the effect of roundedness on perfectly wetting liquids, but also for a liquid with nonzero contact angle the roundedness leads to a certain restriction on r. We derived this restriction in the form of a limitation on Ro from geometrical reasoning as illustrated in figure 3.b. At fixed θ liquid radius r cannot become smaller than the radius with which it is coinciding with the corner radius at the capillary walls. Using the sine rule and conversion rules from sine to cosine this leads to the following geometrical limitation on Ro:

$$Ro_{max} = \frac{r_0}{r_{min}} = \frac{\cos(\theta+\alpha)}{\cos\alpha} \quad (6)$$

This restriction makes it possible to determine the minimum radius of curvature r_{min}, at which the films break up from the surface and its corresponding most negative h value h_{min} by the YL equation. It shows that for liquids with smaller contact angle θ smaller curvatures r are possible.

Liquid distribution through a cross section of the capillary can be related to liquid radius of curvature r leading to expressions for the liquid filled area. r at a certain suction h can be found through the YL equation (1) which in turn determines the liquid filled area of a capillary cross section A(r) which is proportional to r^2. A(r) constitutes of the sum of the cross sections of all four liquid corner films. The total cross sectional area of the capillary is defined as A^{tot}. Equations 7 and 8 give A^{tot} and $A(r)$:

$$A^{tot} = d^2 - F_n\,(0)\,{r_0}^2 \quad (7)$$

$$A(r) = F_n\,(\theta)\,r^2 - F_n(0)\,{r_0}^2 \quad (8)$$

Here it is assumed that the circle inscribing the rounded corner has a contact angle θ of zero with the capillary wall as is the case in figure 3 a and b. F_n is an angularity factor that comes from geometrical considerations and for a square capillary is given by:

$$F_n(\theta) = 4(\cos\theta^2 - \sin\theta\cos\theta - \frac{\pi}{4} + \theta) \quad (9)$$

By the YL equation all areas can be related to h.

2.2 Viscous effects: Flow through corner films

During stage 1 of evaporation the liquid can be transported by advection through the volume of the corner films. For flow to occur the capillary gradient from main meniscus to surface has to overcome the opposing gravity force and pressure drop along the flow path due to viscous losses. The liquid flux through each cross section of a film can be related to the total pressure gradient resulting from capillary and gravity forces and the friction of the liquid with the capillary walls. Ransohoff and Radke [18] derived from the equations of motion for incompressible, Newtonian liquids, expressions that describe the average velocity of liquid in corners bounded by a liquid-gas interface. Their derivations lead to a general solution for average velocity $\bar{v}$ through a corner film cross section which is slightly adapted here to also account for different configurations of the capillary by introduction of inclination angle φ. φ gives the angle between flow direction and the horizontal plane and thus represents the component of the gravity force that opposes flow. The average velocity through a corner cross section is then given by:

$$\bar{v} = -\frac{\rho g r(h)^2}{\varepsilon(h)\,\eta_0}\left(\frac{dh}{dz} + sin\phi\right) \quad (10)$$

Where η_0 is the dynamic viscosity of the liquid and ε is a dimensionless resistivity factor which is constant in the case of a sharp corner. ε for rounded corners however becomes a function of roundedness and increases in a highly nonlinear way with Ro. This can be understood as follows: with decreasing r the liquid film thins and behaves more like a thin film along the corner wall leading to increased resistances. This effect was studied by Ransohoff and Radke [18] who derived numerical results of ε as a function of Ro from the equations of motion for Newtonian incompressible fluids with low Reynolds number. Their calculations give results on the effect of Ro, α and θ on ε. Zhou et al. [20] derived approximate analytical solutions of ε as a function of Ro, with the parameters α and θ included, for the two cases of no flow or a free boundary at the liquid/gas interface. The type of boundary taken affects the length of the wetting boundary that generates flow resistance. Results of both are compared in Chauvet et al. [17] for square capillary and perfectly wetting fluid and are very similar. For our corner flow model we will use the analytical solutions of Zhou because they provide a

way to calculate ε for each value of Ro taking into account the contact angle θ as well. We make the assumption of a free boundary at the liquid/gas interface which gives the following expression of ε [20]:

$$\varepsilon = \frac{12 \sin\theta^2 \alpha (1-B)^2}{(1-\sin\alpha)^2 B^2} * \frac{(\psi_1 - B\psi_2)(\psi_3 - (1-B)Ro)^2}{(\psi_1 - B\psi_2 - (1-B)Ro^2)^3} \quad (11)$$

Constants ψ_1, ψ_2, ψ_3 and B are dependent on the corner half angle α and liquid contact angle θ and are defined as in equations (12-15):

$$\psi_1 = \cos(\alpha+\theta)^2 + \cos(\alpha+\theta)\sin(\alpha+\theta)\tan\alpha \quad (12)$$

$$\psi_2 = 1 - \frac{\theta}{\pi/2 - \alpha} \quad (13)$$

$$\psi_3 = \cos(\alpha+\theta)/\cos\alpha \quad (14)$$

$$B = (\frac{\pi}{2} - \alpha)\tan\alpha \quad (15)$$

Note that ε can easily be rewritten as a function of h by applying the Young Laplace equation to the expression of roundedness Ro.

2.3 Characteristic length

The depth at which the corner films break up from the surface is defined as the characteristic film length L_c. It is a result of both gravity and viscous losses opposing capillary force which leads to break-up as soon as the first two exceed the capillary driving force. We therefore start with defining a characteristic length for the simplified case where only gravity force is opposing capillary force for a vertically orientated capillary. This corresponds to a hydrostatic force balance where the height of the liquid z above a zero pressure level equals the absolute value of h and is thus directly related to the liquid curvature r. We define the characteristic length for this case as the gravity length L_G which is equal to the difference between absolute values of snap off suction h_d at the main meniscus and

maximum absolute value of h at the surface limited by r_0. The gravity length is increasing with decreasing corner radii because higher suctions can be reached before the curvature radius of the film equals the corner radius.

In the same way as for the gravity length it is possible to define a characteristic viscous length L_V that corresponds to the maximum film length if only viscous losses would oppose capillary force. This is the case for a horizontal capillary with inclination angle φ equal to zero. L_V depends on flow rates and thus decreases with higher evaporation rates. The characteristic length L_C results from a combination of L_G and L_V.

2.4 Modeling strategy and simplifications

A modeling approach was developed to predict characteristic film lengths L_C that can be compared to experimental results. The corner flow model is first of all based on the assumption of a constant flux at the capillary surface as long as the corner films extent up to the surface. This means we assume a stage 1 with constant drying rates measured over the whole area of the capillary for the duration of intact films up to the surface. It is also assumed that evaporation is only occurring from the tips of the films, and diffusion from liquid/gas interface inside the medium is negligible due to small vapor concentration gradients inside the capillary. This is reasonable since the vapor concentration inside the capillary will everywhere be close to saturated vapor concentration.

These assumptions lead to a mass balance requirement of a constant flux through each cross section of the corner films that equals the initial flux at the surface. However as the main meniscus moves down and the films become thinner the liquid flowing from meniscus to capillary surface experiences more resistance and at some depth it is not possible to sustain the required flux. This then leads to breakup of the films and defines the maximum film length L_c.

The constant flux requirement can be expressed as follows:

$$e_0 \, A^{tot} = \bar{v}(r) \, A(r) \tag{16}$$

Where e_0 is the initial evaporation rate in mm/d, A^{tot} and A(r) are the total cross sectional area of the capillary and the liquid filled cross sectional area above main meniscus respectively as described by equations 7 and 8. $\bar{v}(r)$ is the average velocity of the liquid in mm/d at a certain cross section as given by equation 10.

The left hand side of equation 16 defines the initial mass flux from the capillary and is a constant value. Inserting (8) and (10) into (16) and rewriting r and ε to h by use of equation (1) leads to the following equality:

$$e_0\, A^{tot} = -\frac{1}{\varepsilon(h)}\left(\frac{F_n(\theta)\sigma^4}{\eta_0(\rho g)^3}\frac{1}{h^4} - \frac{F_n(0){r_0}^2\sigma^2}{\eta_0\rho g}\frac{1}{h^2}\right)\left(\frac{dh}{dz} + sin\phi\right) \tag{17}$$

In equation 17 all terms are either constant or a function of h which means that a separation of variables can be performed. When the meniscus depth z_m equals L_C the corner films break. The depth z thus has to be integrated between z=0 at the surface to z=L_C at the meniscus. The integration boundaries of h are defined by most negative head value h_{min} at the surface of the capillary and h_d at the main meniscus. This means that all integration boundaries are known leading to the following expression for L_C:

$$\int_{h_{min}}^{h_d} \frac{dh}{\frac{\varepsilon(h)e_0\, A^{tot}}{\left(\frac{F_n(\theta)\sigma^4}{\eta_0(\rho g)^3}\frac{1}{h^4} - \frac{F_n(0){r_0}^2\sigma^2}{\eta_0\rho g}\frac{1}{h^2}\right)} + sin\phi} = L_c \tag{18}$$

For rounded corners this equation can only be solved numerically because ε becomes a function of h leading to a complex integral. However for sharp corners ε has a constant value and the following analytical solution can be found:

$$L_C = \sum \frac{2\,\mathrm{ArcTan}\left[\sqrt{\frac{2c_0}{c_{2h}\,\mathrm{Sin}[\varphi] - C_{all}}}\,h\right]\left(2c_{4h}c_0 - c_{2h}^2\,\mathrm{Sin}[\varphi] + c_{2h}C_{all}\right)}{\sqrt{8c_0\,{C_{all}}^2 c_{2h}\,\mathrm{Sin}[\varphi] - 8c_0{C_{all}}^3}}$$
$$+ \frac{2\,\mathrm{ArcTan}\left[\sqrt{\frac{2c_0}{c_{2h}\,\mathrm{Sin}[\varphi] + C_{all}}}\,h\right]\left(c_{2h}^2\,\mathrm{Sin}[\varphi] - 2c_{4h}c_0 + c_{2h}C_{all}\right)}{\sqrt{8c_0{C_{all}}^2 c_{2h}\,\mathrm{Sin}[\varphi] + 8c_0{C_{all}}^3}} \tag{19}$$

423 with the constants defined as follows:

$$C_{all} = \sqrt{c_{2h}^2 \, \mathrm{Sin}[\varphi]^2 - 4 c_{4h} c_0 \, \mathrm{Sin}[\varphi]}$$
$$c_0 = \varepsilon_h \, e_0 \, A_{tot}$$
424 $$c_{4h} = \frac{F_n \sigma^4}{\eta (\rho g)^3}$$
$$c_{2h} = -\frac{F_n r_0^2 \sigma^2}{\eta \rho g} \qquad (20)$$

425 Solving gives L_C as a function of initial evaporation rate e_0, capillary orientation ϕ and width d, corner
426 radius r_0 and liquid properties.

427 3. Experimental methods

428 Experiments are done on evaporation of the liquids ethanol and water from two different sized glass
429 capillaries with square cross section (supplier: Vitrocom). The two liquids are chosen to investigate
430 the effect of different liquid properties like σ and θ. In some of the experiments blue dyed liquids are
431 used to visualize locations of phase change that are indicated by dye deposition on the capillary
432 walls. This allows for validating whether the underlying modeling assumption of phase change only
433 happening at the top of the corner films is true.

434 Two sizes of capillaries are used of width d equal to 1.0 and 0.5 mm respectively. From high
435 magnified images of the top of the capillaries the corner radii are determined giving an r_0 for the
436 large (d=1.0 mm) capillary of 90 µm and for the small (d=0.5 mm) of 58 µm. Figure 4 shows a photo
437 of the experimental setup. The capillary is glued on a syringe containing the evaporating liquid which
438 in turn is placed on a high precision pump. This allows for accurate filling of liquid to the top of the
439 capillary and fixing its position. From this point on evaporation takes place from the top which is
440 open to the atmosphere.

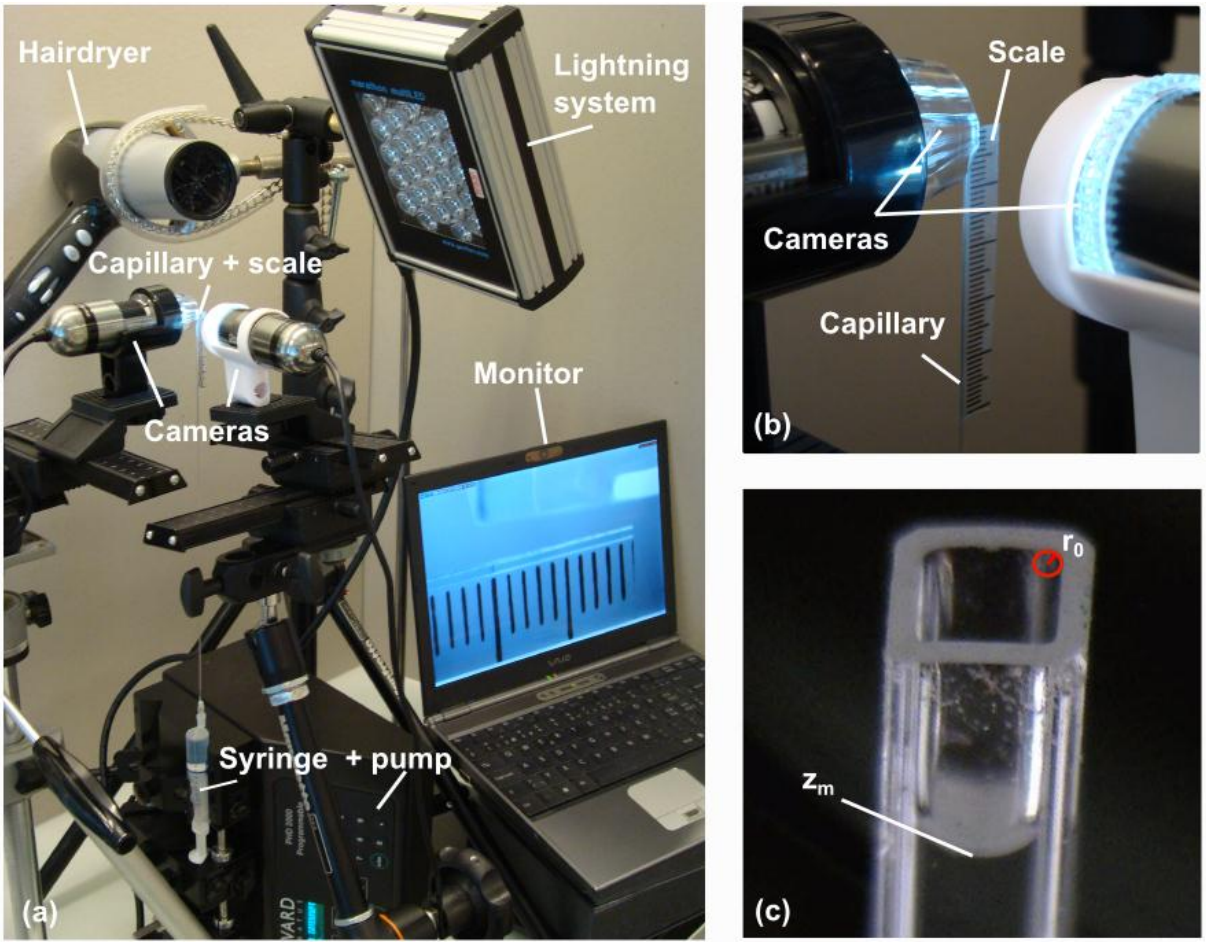

442 *Figure 4: a) The experimental setup with the capillary attached to a syringe which is placed on a high*
443 *precision pump. A hairdryer is used to vary external demand leading to different evaporation rates. b)*
444 *Two microscope cameras image corner films and the movement of the main meniscus. The capillary is*
445 *in between these cameras with a length scale attached to it. c) A high magnified image of the*
446 *capillary (d=1.0 mm) with the main meniscus position z_m and corner films above. The corners are*
447 *slightly rounded with corner radius r_0 of 90 µm.*

448 Two microscope cameras (Dinolite, resolution 1280*1024 or higher) are directed to the capillary.
449 One is positioned such that it monitors one capillary wall with its two adjacent capillary corners
450 under high magnification at the top of the capillary, to visualize the evolution of the corners and their
451 break-up from the surface. The second camera, positioned at an angle of 90 degrees with the first
452 one, monitors the capillary at lower magnification to visualize depth of the main meniscus with time.
453 Depending on the magnification rate of this second camera break-up of a third corner film could

454 often be seen. Thus by use of both microscope cameras the characteristic length of maximum three
455 of the four liquid films could be determined.

456 Figure 5 shows two high magnified images of the top of the capillaries for ethanol and water at the
457 moment that the main meniscus is moving into the medium while liquid remains trapped in the
458 corners. An inscribed circle of the meniscus interface shows the difference in contact angle for both
459 liquids. For ethanol θ is 0° (perfectly wetting liquid) while for water θ is around 30°. This is an
460 important difference between the two which influences drying dynamics. Other liquid properties are
461 summarized in table 1.

462 To investigate the significance of viscous losses on L_C a range of different evaporation rates are
463 applied by directing a hairdryer on the capillary with different strength. Only cold air is used to
464 exclude thermal effects on evaporation and liquid properties. In fact we assume an isothermal
465 system where we do not take into account the cooling effect of phase change from liquid to vapor at
466 locations where evaporation occurs. Chauvet et al. [17] state that this cooling was at most 2.5 K for
467 2-propanol in their experiments which is small enough to assume an isothermal system. Gravity
468 influence is varied by positioning the capillary under different inclination angle ϕ. Horizontal, vertical
469 and an angle of 30° are used.

470

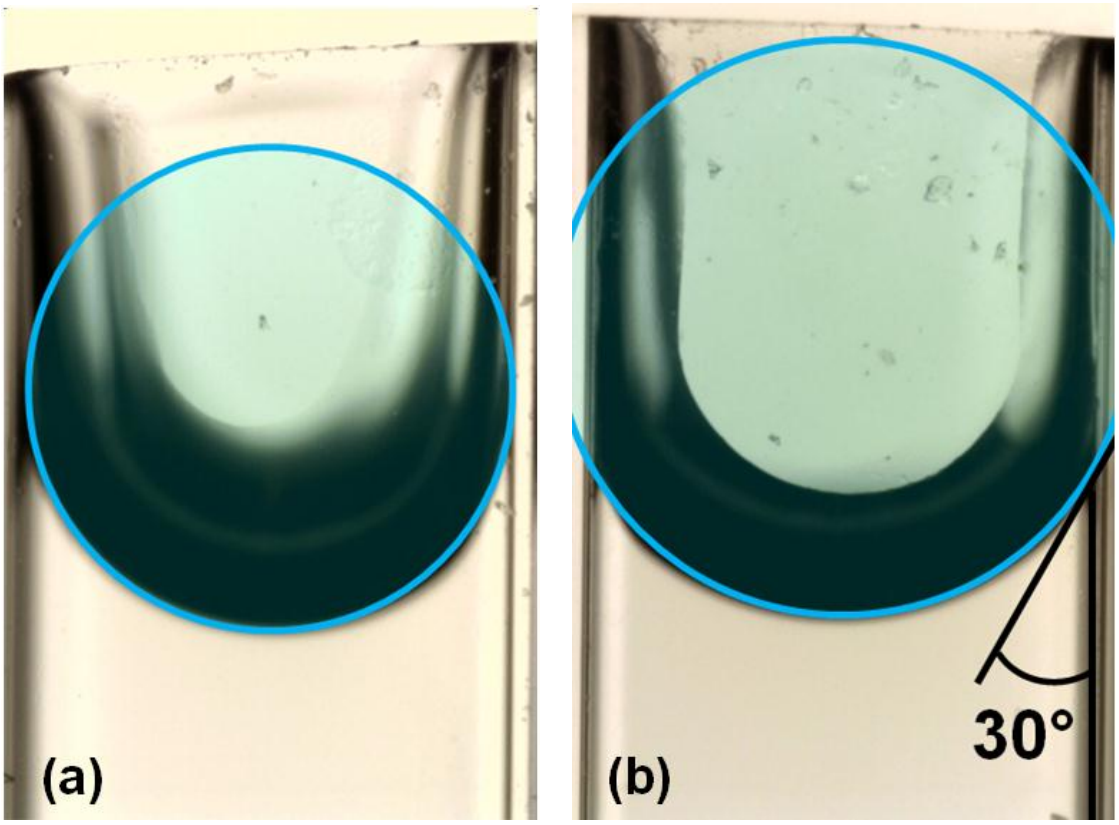

Figure 5: Two high magnified experimental images of the receding menisci of a) ethanol and b) water showing the difference in contact angle (ϑ=0 for ethanol, ϑ= 30 degrees for water) as highlighted by the inscribed circle that fits to the interface of the main meniscus. Evaporation from the top of the capillary (top of the images) leads to downward movement of the meniscus and the formation of liquid films in the corners. These images show one capillary wall (d=1.0 mm) with its two adjacent capillary corners.

	ethanol	**water**
Density ρ (kg/m^3)	789	998.21
Surface tension σ (N/m)	0.02239	0.0728
Dynamic viscosity η_0 (kg/(m*s))	0.00107	0.001002
Vapor pressure (Pa)	8000 (at T=298 K)	2800 (at T=298 K)
Contact angle	0°	30°

Table 1: Liquid properties of ethanol and water.

Evaporation rates e can be deduced from photos of the microscope camera that images main meniscus position z_m at either 20 or 10 seconds time intervals for slow and fast evaporation experiments respectively. A scale is attached to the capillary to determine equivalent length of one pixel. By image analysis in Mathematica z_m could then be determined for each imaged time step.

Accurate measurement of drying rates is important since the initial evaporation rate e_0 of the experiment is one of the input parameters of the proposed model. Dividing the change of two subsequent meniscus positions dz_m by their time difference gives meniscus velocity $\frac{dz_m}{dt}$. This is converted to an evaporation rate by the simplifying assumption that for a change in meniscus position dz_m the evaporating liquid area is equal to the gas filled area at the snap off suction h_d. Therefore the volume V_e of liquid evaporated in time step *dt* equals

$$V_e(t) = dz_m(t) * (A^{tot} - A(h_d)) \quad (21)$$

The evaporation rate *e(t)* is then given by:

$$e(t) = \frac{1}{A^{tot}} \frac{dVe}{dt} \quad (22)$$

4. Results

For all experiments it was possible to monitor detachment of at least two of the total four corner films because these were monitored by the microscope camera with largest magnification. Depending on the magnification of the second camera which monitored the evolution of z_m, detachment of a third corner film could be seen. For nondyed liquid the moment of detachment of corner films could be easily determined from photos. Maximum film extent could vary for the different corner films of one experiment which can probably be attributed to slight variations in the corner radii of the different capillary corners. Model results show that depending on which e_0 is taken into consideration a small change in r_0 can have a significant effect on L_C values. If the corner radius of 90 µm as determined for the large capillary changes with 1 % it leads to a change in L_C of 12 % for an e_0 of 500 mm/d, ethanol evaporation and vertical configuration.

503 Experiments indicate that the evaporation and corner film dynamics for ethanol and water showed
504 very different behavior. Figure 6 shows a typical evolution of the main meniscus with time for both
505 liquids with the break-up depth indicated by the grey shaded area. For ethanol evaporation, L_C values
506 for different corners in one experiment lie close together as indicated by the narrow band in fig. 6.a.
507 representing break-up depth which lie between 11.1 and 11.4 mm in this case. For water however
508 different corner films can have a large variation in break-up depth for one experiment as shown in
509 figure 6.b. by the broad shaded area varying in this case between 4.9 and 8.3 mm.

510 Also qualitatively it could be seen that the films behave in a different way. In the case of ethanol they
511 get loose at the surface and then retreat in a more or less smooth way into the capillary while
512 remaining present but moving down with the main meniscus. For water they tend to break-up
513 between surface and meniscus after which the film above the break-up point evaporates and
514 disappears. While the meniscus moves down a new film can stretch out inside the capillary, which
515 later might break again and disappear.

516 The evolution of z_m for both liquids has in common that after film break-up the movement slows
517 down as can be seen from a decrease in slope in fig. 6. This can also be seen in evaporation rates as a
518 function of z_m as shown in figure 7 for ethanol and in figure 9 for water. For water break-up depth are
519 always smaller than for ethanol, which can be explained by the contact angle that poses a tighter
520 restriction on h at the surface of the capillary, since the films will detach already at larger curvature r.

521 The insets of figure 6 show the high magnified images of the top of the capillary at different
522 moments of the experiment. In fig. 6.a. images show distribution of undyed ethanol before and after
523 film break-up where the liquid phase is indicated by the blue shaded area. The first inset shows two
524 corner films extending to the capillary surface and the main meniscus whereas the second shows a
525 smaller section of one capillary corner with the film tip that retreated inside the capillary. The tip of
526 the film is indicated with a red arrow. In figure 6.b. images of undyed water are shown, with the
527 break-up of left and right corner film in respectively the second and third image shown in more

528 detail. In this case the left film did not break up at the surface but instead somewhere halfway the
529 film. Also break-up of these two different films in one experiment happened at very different
530 moments.

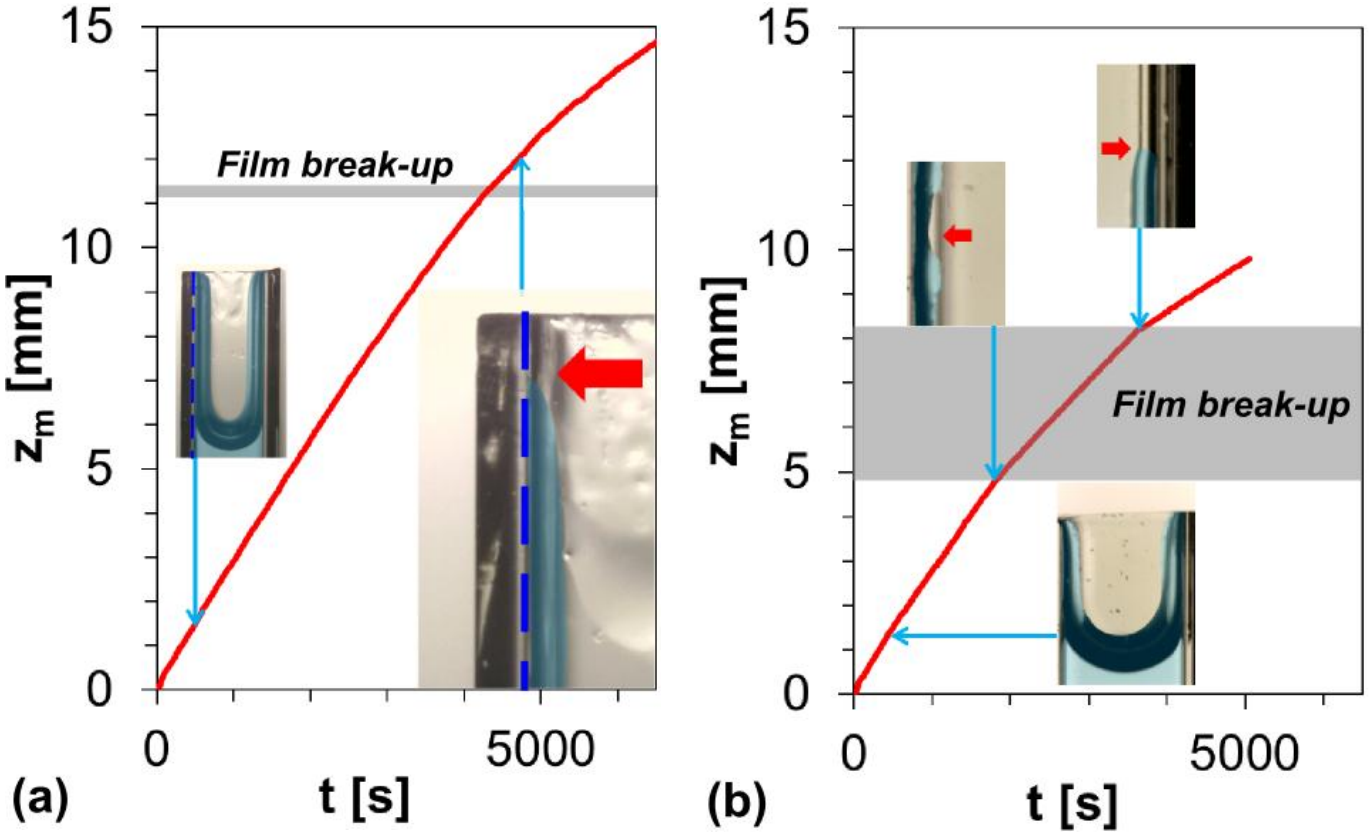

531

532 *Figure 6: Evolution of depth of the main meniscus z_m with time for single experiments of evaporation*
533 *from a vertically orientated capillary (d=1.0 mm) for ethanol (a) and water (b). The gray band shows*
534 *the range of z_m at which the different cornerfilms break. For ethanol they lie close together with*
535 *values of 11.1 to 11.4 mm,whereas break-up depths for water show a much larger variation of 4.9 to*
536 *8.3 mm. After break-up the slope decreases which corresponds to lower evaporation rates. The insets*
537 *show high magnified images of the top of the capillary showing the liquid distribution (blue shaded)*
538 *at different moments of the experiment for a)undyed ethanol and b) undyed water. Red arrows show*
539 *the breakup point of the cornerfilm.*

540 Figure 7 shows the evaporation rate versus z_m for different experiments with ethanol highlighting the
541 effect of increased viscous resistance for higher flow rates in (a) and the effect of gravity in (b). 7.a.

shows the evolution of z_m for two experiments differing in their external evaporative demand leading to different initial drying rates e_0. The blue line in 7.a. shows evaporation rates for an e_0 of 1080 mm/d while the red one had an e_0 of 220 mm/d. The meniscus depth at which films breakup is indicated by the change from solid to dashed line. Increased e_0 has a clear effect on break up depth L_c of the films. For the high evaporation rate films break up at 8.6 mm, while for the lower e_0 L_C is 11.1 mm. This is a result of increased viscous losses with increasing evaporation rates and the resulting higher flow rates through the corner films that lead to a reduction in L_c. In Figure 7.b. the effect of the magnitude of gravity opposing the capillary force is shown. The blue curve represents the same data set for vertical configuration as the blue curve in fig. 7.a. while the red line shows the results for a horizontal configuration. The initial evaporation rates for both experiments are similar,e_0=1080 mm/d and 950 mm/d for blue and red data respectively. However the break-up depth of the horizontal experiment is much larger with its 43 mm as opposed to 8.6 mm of the blue curve, showing the effect of decreasing gravity influence.

In both graphs of fig. 7 a time compression analysis of the red data sets is shown. In such analysis $\frac{1}{e^2}$ is plotted against time t where the graph is horizontal for advection dominated transport and becomes linearly increasing as soon as diffusion is the dominant transport mechanism in stage 2 [23]. This way the moment where diffusion becomes dominant could be derived from the bent of the graph. This moment corresponds with the moment of film break-up for the experiments. Note however that in all experiments evaporation rates already start dropping before breakup of the films.

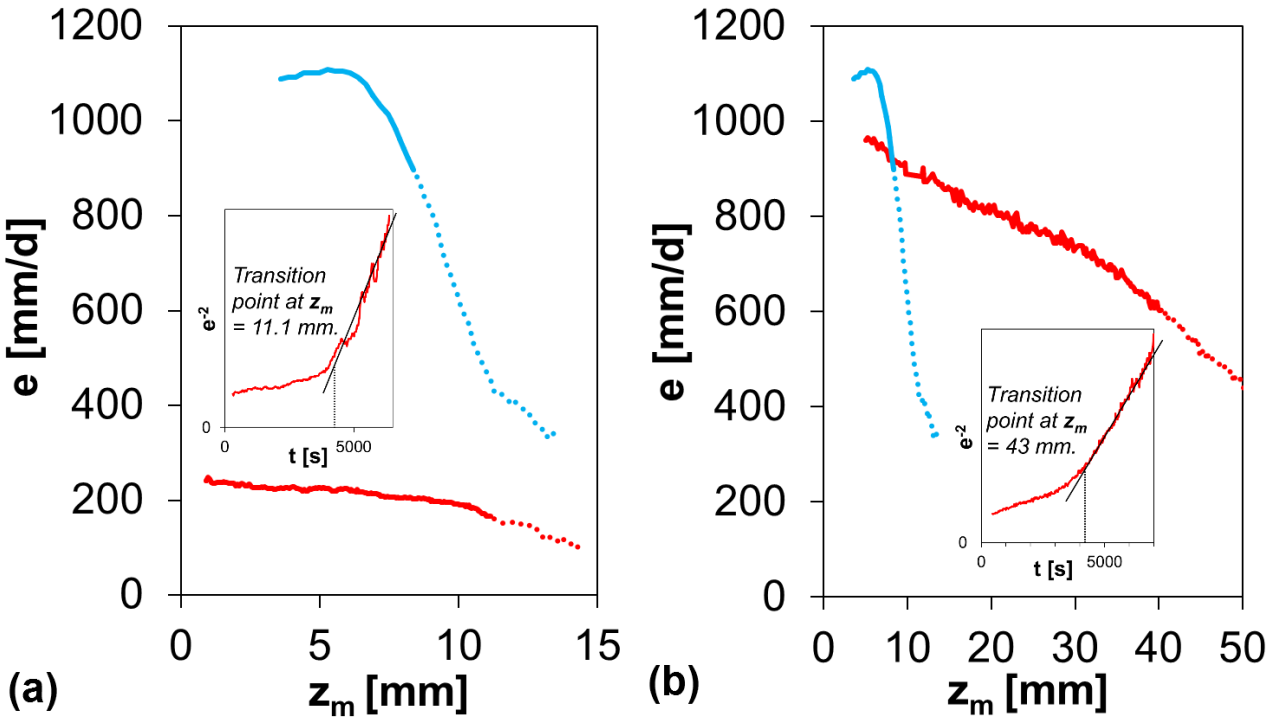

Figure 7: Evolution of evaporation rate e with depth of the main meniscus z_m for different experiments of ethanol evaporation from a capillary of d=1.0 mm. The transition between continuous and dashed line represents the depth of cornerfilm detachment L_C. Insets show a time compression analysis for the red data sets where a clear bend in the slope indicates the transition to diffusion dominated transport after which the line becomes approximately linear. From comparison with the moment of film break-up it is found that this transition occurs at film break-up. Left figure shows measured e for two vertically orientated experiments but different initial drying rates e_0 of 220 mm/d (red) and 1080 mm/d (blue). L_C decreases for increasing e_0 from 11.1 to 8.6 mm. Right figure shows the effect of capillary configuration for two experiments with φ=90° (blue) and φ=0° (red) and similar e_0 of 1080 mm/d (blue) and 950 mm/d (red). L_c changes from 8.6 to 43 mm for vertical and horizontal case respectively showing the effect of gravity.

Figure 8 shows a comparison between model predictions of ethanol as well as the experimental results for L_c plotted against e_0. Solid lines and markers are indicative for respectively model outcome and experimental results. On the vertical axis L_C is scaled to the gravity length L_G for the respective capillary size in vertical orientation. L_G follows from the difference between suction at the main

meniscus and at the surface where the latter is determined by r_0. This leads to theoretical values of L_G of 21.3 mm for the large capillary and 28.1 mm for the small. Blue and red series give results for a vertical orientation (ϕ=90°) of the large capillary (d = 1mm) and small capillary (d=0.5 mm) respectively. The green series gives the result for ϕ=30° and the yellow for a horizontal configuration (ϕ=0°), both for the large capillary.

For the error bars in the experimental results the standard deviation of different break-up depths of the respective experiment is taken into account. The marker indicates the mean of all corner films for which detachment could be monitored in this experiment. For the horizontal case error bars are larger which is not because the range of break-up depths in different corners is larger, but because the moment of break-up is more unclear in the high magnified images for such orientation. In a horizontal case the gravity influence which has a stabilizing effect on the films is absent. In this case films become increasingly thinner over a wide range of z_m while it can be seen from increased formation of air bubbles along the films that diffusion from inside the medium is becoming increasingly significant at the same time. We can thus argue that there is a larger transition time between advection dominated and diffusion dominated transport where during this transition both transport mechanisms are significant. This can be explained by the fact that under zero gravity component opposing the films there is no force pulling them inside the capillary. The viscous losses only lead to decreasing flow rates inside the films while diffusion can become important as well. In this horizontal case the moment of detachment was derived from photos of the moment that films got significantly thinner and a time compression analysis of the drying rates.

Model predictions and experimental results coincide very well. Only the yellow series shows some significant deviation from the model predictions for a horizontal configuration. This is probably due to the fact that for small ϕ a slight change in the significant gravity component has a large effect on L_c. For an absolutely horizontal case L_c can in theory become infinity when there are no viscous losses which is the case when there is no evaporation. However a slight change in angle adds the gravity component which immediately defines a finite value for L_g. Therefore the model predictions for ϕ=1°

604 are included by the yellow dashed line, showing that the experimental results fall inside these two
605 predictions.

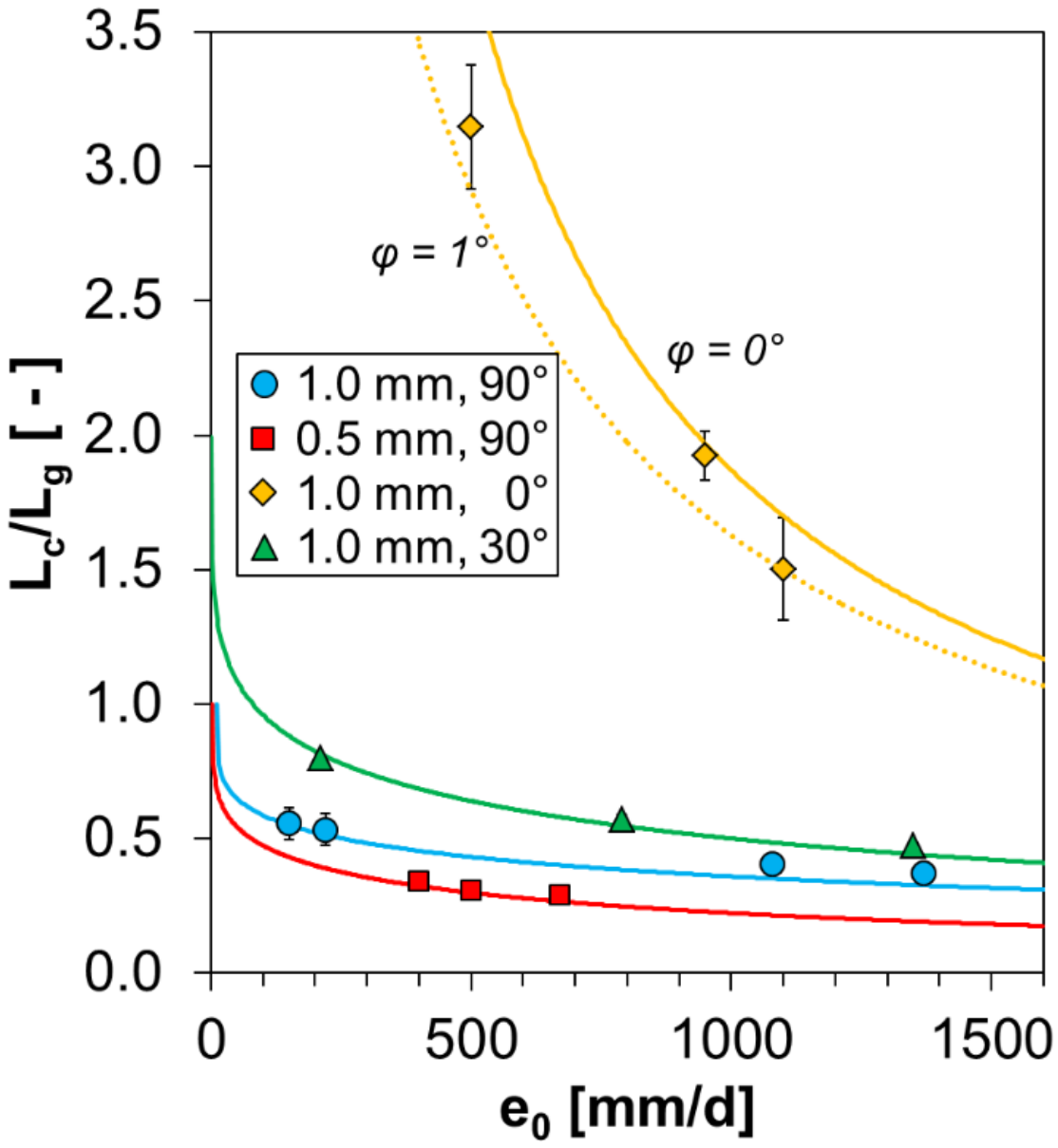

606

607 *Figure 8: Comparison of experimental and model results. L_C on the y axis is scaled to the calculated*
608 *value of gravity length L_G where L_G=21.3 mm for large capillary (d=1.0 mm, r_0=90 µm) and 28.1 mm*
609 *for small capillary (d=0.5 mm, r_0=58 µm) respectively. Markers and solid lines indicate experiments*
610 *and model predictions respectively for different capillary orientations of φ=0, 30, and 90°. The dashed*
611 *yellow line gives model predictions for φ=1° (d=1.0 mm). L_c decreases with increasing e_0 and*
612 *increasing φ.*

As stated earlier water behaved very different from ethanol during evaporation experiments from the large capillary (d=1.0 mm). Films often did not break up at the surface of the capillary, but instead closer to the meniscus. Furthermore the break-up of different corner films in one experiment showed a large variation. Figure 9.a. shows evaporation rates versus time averaged from three different experiments with similar e_0 around 200 mm/d of water evaporation for large capillary. This averaging was done to smooth out the irregular behavior of water in the different experiments. The black line indicates the average break-up depth of the corner films where the blue shaded area has a width of two standard deviations as determined from all different corner film break-up depths of these three experiments. It can still be seen that after film break-up drying rates show a significant drop. Figure 9.b. shows predictions of the corner flow model for film break-up of water taking into account the effect of nonzero contact angle θ on resistivity factor ε as well as on the limit of r at the surface due to the rounded corner. Model predictions as well as experimental results are shown for two different ϕ and large capillary. Experimental results deviate significantly from the model predictions and the experiments do not show a trend of decreasing L_C with increases in e_0 and ϕ. We can only say that the order of magnitude of model predictions and experimental results are in agreement.

This complex behavior can mainly be explained by the nonzero contact angle. Changing the contact angle from 0 to 30° changes both upper and lower integration boundaries h_d and h_{min}, reducing the whole integration range with increasing θ. For the large capillary (d= 1.0 mm, r_0= 90 µm), θ=0 and ethanol liquid properties the integration boundaries are h_d=-10.9 cm and h_{min}=-32.1 cm, while for θ=30° and water properties the integration range is reduced to h_d=-23.8 cm and h_{min}= -30.2 cm. Here h_d is calculated by equation 4 and h_{min} by implementing r_{min} from equation 6 in the Young Laplace equation. This poses a tighter mechanical range for water over which the films can exist, which means that before L_c comes into the viscous limited range, it is already breaking up due to these mechanical restrictions. This can be seen in the fact that in figure 9.b. the model predictions for L_c only show a small declining trend with increasing e_0. However the restriction to r at the top of the

capillary as stated in the model and in equation 6 deviates from reality. This is because close to the top of the capillary the second direction of the radius of curvature becomes important because the system adjusts to the singularity of the film tip at the surface. From the experimental images it can be seen that at the top of the films the second radius of curvature has a different sign than the main one. This means that the main radius of curvature r becomes equal to r_{min} already at lower suctions than if this second radius is not taken into consideration. Thus the range of suction values at which the films can exist becomes even smaller and this would lead to earlier film break-up in the experiments than as predicted by the model. This is the case for most experimental results in figure 9.b. However since in this case the geometry of the corner is so restrictive to L_c slight variations in its corner radius r_0 have a large effect on L_c. In other words, the break-up depth of the corner films is highly sensitive to corner radius variations and other mechanical irregularities. Thus to study the viscous effect on water corner films, a different capillary should have been used to provide for larger suction range.

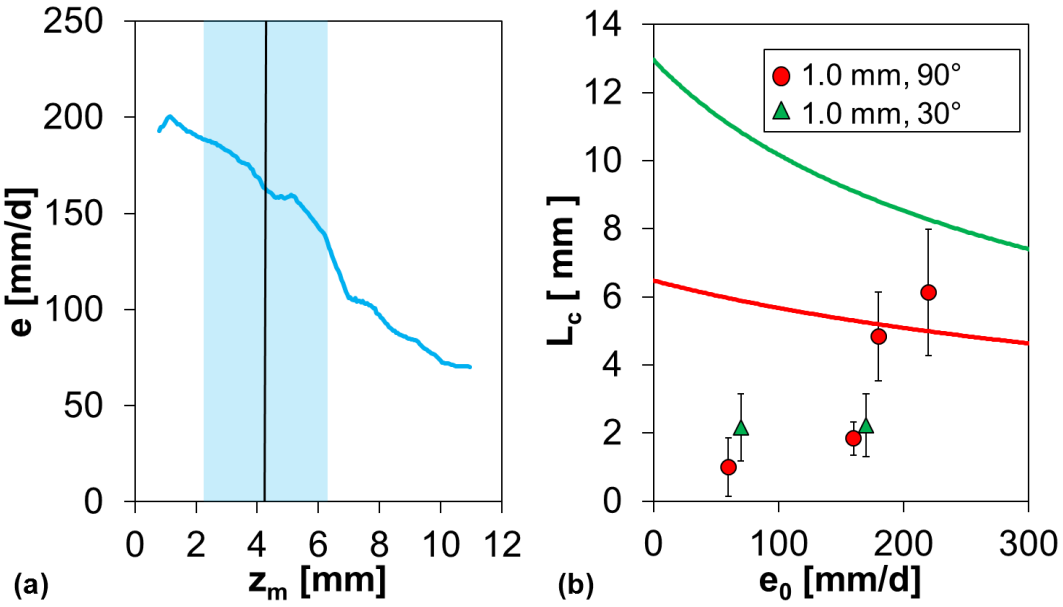

Figure 9: Results for evaporation of water from large capillary (d=1.0 mm). a) shows the evolution of drying rates composed of the average values of three similar experiments with identical e_0 to smooth out the irregular behavior of water. The blue area represents the range of film break-up of different corners, with the average represented by the black line and the width equal to two standard

deviations. After break-up of all films drying rates show a significant drop. b) shows a comparison of experimental results (symbols) and model predictions (solid lines) of L_C for two different capillary orientations (φ=90° and 30°). Clearly water has a complicated behavior that is not reflected in the model predictions. (L_G for the large capillary and water characteristics is 6.5 mm).

5. Discussion

5.1 Effects of gravity and viscous losses on L_C

The gravity effect on L_C was studied by changing the inclination angle ϕ of the capillary giving results for 3 different orientations as shown in figure 8.The horizontal configuration leads to the largest L_C values since in this case only viscous losses are opposing capillary force. Model result for this configuration predicts an infinite length if there is no evaporation since in such a case neither gravity nor viscous losses oppose the capillary force. A vertical configuration leads to smallest L_C values because the component of the gravity vector opposing capillary force is maximum in this case. With decreasing initial evaporation rates the L_C values for vertical orientation approach gravity length L_g. For the case of ϕ=30° sin(ϕ) equals 0.5, leading to a gravity component opposing flow which is half the one in the vertical case. Therefore L_C becomes twice L_G for e_0 equal to 0 with this orientation.

Viscous losses become more significant with increasing e_0 since mass flux through the corner films increases leading to higher resistance to flow. Because of increasing viscous effects model predictions show a decreasing trend of L_C with increasing e_0 for all capillary configurations. Experimental results correspond well to these model predictions and also show a decreasing trend with increasing evaporation rates. The effect is most pronounced for the horizontal case since here L_C is only determined by viscous losses due to flow. The experimentally determined L_C for e_0 of 500 and 1100 mm/d decreases roughly with a factor of 2 from 67 mm to 32 mm in this case.

5.2 Effect of capillary geometry on L_C

Two different capillary width d were used in the experiments with the initial aim to investigate the effect of different capillary sizes. However the corners of the capillaries are slightly rounded where r_0 of the large capillary is significantly larger than that of the small one, 90 opposed to 58 µm. As discussed r_0 has a large effect on L_C by firstly creating a limit on h at the surface, and secondly by affecting the resistivity to flow, where the resistivity increases in a highly nonlinear way as the corner films become thinner. Because of these nonlinear effects it is not possible to make a general statement about the difference between small and large capillary. The smaller r_0 at the surface as well as the smaller total capillary area leads to a different range of possible head values and integration boundaries. The average thickness of the films for the small capillary is smaller due to higher suctions which leads to smaller areas through which the liquid has to move, and thus more flow resistance. On the other hand due to the smaller r_0 of the small capillary the resistivity factor ε for thinner films is not as high as for the larger r_0 of the large capillary.

To have a simplified idea of influence of capillary size we can still make some hypothetical discussion about this effect if the corners would have been sharp. The easiest situation to look at size effects is the horizontally orientated capillary where only viscous losses are limiting the corner film length. Capillary width d first of all influences h_d and thus the range of suction values over which the corner films exist. Since h_d is inversely proportional to width d and the ratio of large to small capillary we used is 2, it is twice as large for the small capillary. L_C follows from integration over the range of h values from meniscus to surface which means this would have an effect on L_C. For the more negative h values the films become thinner and resistance to flow increases. The relative importance of the viscous losses thus becomes higher for smaller capillaries and this would have a decreasing effect on L_C with decreasing d. On the other hand the total cross sectional area of the capillary decreases with decreasing d which means that the total flux that must be sustained through each cross section of the corner films becomes smaller for the same initial evaporation rate e_0. This has an increasing effect on L_C with decreasing d. For a sharp corner ε is a constant and for the case of ϕ equals 0 the integral of equation 18 reduces to:

$$\int_{-\infty}^{h_d} \frac{F_n(\theta)\sigma^4}{\varepsilon\, e_0\, A^{tot}\eta_0(\rho g)^3 h^4} dh = L_v \sim [\frac{1}{A^{tot}}\ \frac{1}{{h_d}^3}] \quad (23)$$

This means that with a ratio of 2 of large to small capillary the length becomes twice as small for the smaller capillary. Thus the increased resistance to flow in the films of the smaller capillary is a stronger size effect than the decreased flux through the films when ε can be taken constant.

When gravity comes into play it becomes more complicated to predict the effect of capillary sizes since the increased range of head values for the larger capillary also leads to a larger mass in the corner films which has a shortening effect due to gravity acting on this extra mass.

5.3 Patterns of dye deposition

Experiments of evaporation of blue dyed ethanol served to get more insight into the locations where evaporation, the phase change from liquid to vapor, is taking place. One of the main assumptions of the model is that these phase changes only happen from the top of the films as long as these are present up to the surface, and not from inside the capillary. Figure 10 shows two images of the top of the capillary with 10.a. showing the main meniscus, and 10.b. showing the films just before break-up. Dye is deposited on the capillary wall at the locations where liquid goes into the vapor phase leaving a trace of the dye. It is thus an indicator of locations of diffusion. From the high magnified images it could be seen that dye deposition did not only take place at the top of the corner films but also along their boundaries up to a depth inside the capillary of the order of one to two capillary widths. Furthermore dye was deposited on the wall between the two corner films. This is because next to the thick corner films there are also adsorbed thin films on the capillary wall in the case of a perfectly wetting liquid like ethanol. Evaporation of these adsorbed thin films leaves a trace of dye deposited as curved lines above which the wall is completely dry.

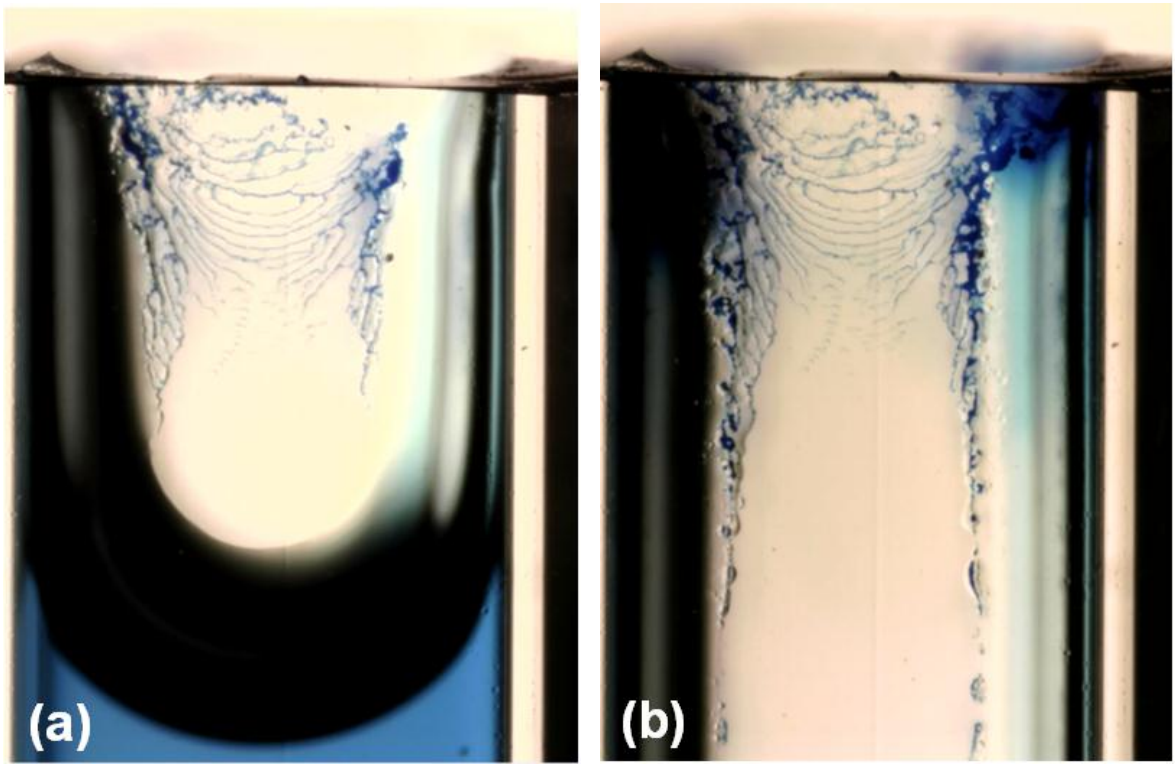

Figure 10: Two high magnified images of dye deposition during ethanol evaporation from a vertically orientated capillary (d=1.0 mm). a. Shows the main meniscus with the corner films extending to the surface. Dye is deposited on the sides of the thick films as well as on the boundary of the thin films of adsorbed liquid on the capillary wall. b. shows an image of the top of the films short before break-up showing that dye is mainly deposited at the top of the films.

Tuller and Or [8]calculated the typical thicknesses of such thin adsorbed films on capillary walls by taking into account van der Waals forces only. They found typical thicknesses of 70 to 0.3 nm for matric potentials for wet and dry conditions respectively. This means they are at least a factor 100 thinner than the corner films, and cannot give a significant contribution to evaporation flux during stage 1.

The fact that dye deposition does take place from inside the capillary while the corner films are still intact shows that it is a simplifying assumption to say that evaporation only takes place from the top of the corner films. In fact the area that we take for the top of the films is not present in reality since close to the capillary surface the second direction of curvature becomes important and at the surface

743 the films only exist in one point. However the good fit of model predictions and experimental results
744 for ethanol of figure 8 shows that it cannot give a large error to make such an assumption.

745 **5.4 Drying rates**

746 In general it could be seen from the drying rate evolution with z_m that drying rates are high in the
747 beginning and start their drop already slightly before film detachment from the surface. Then they
748 drop significantly to much lower drying rates. Such a pattern is similar to the two drying stages of
749 porous media, where the first stage has high drying rates. The high initial drying rates from the
750 capillary can be attributed to advectional transport through the corner films. As soon as the location
751 from which evaporation takes place moves inside the capillary the drying rates become much lower
752 and keep dropping since diffusional distance is increasing.

753 In the first stage of drying before film detachment, rates are not always absolutely constant but often
754 show a slight drop. Therefore initial drying rate e_0, which is a model input, was taken as the average
755 value of the rates in this initial stage before the film break-up. In some cases there was a clear
756 plateau value to which drying rates dropped and then remained more or less constant on this value
757 before film break-up. In these cases this plateau value is taken for initial evaporation rate e_0. For
758 horizontal configuration drying rates were always dropping from the beginning, in this case the initial
759 value at the beginning of the experiment was taken as e_0.

760 The fact that drying rates already start dropping before film detachment means that the model
761 assumption of constant fluxes as long as the films extent to the surface is in fact an
762 oversimplification. This drop in drying rates could be due to limitations by the coupling between the
763 liquid filled patches in the capillary corners and the atmospheric boundary layer above. Since the
764 surface of the capillary is increasingly drying out the liquid filled areas might become too small to
765 sustain the original high drying rate at the beginning of the drying process.

766 As a final note on drying rates it is quite remarkable that rates can have the high values as
767 determined from the experiments. We can make some calculations to show that these drying rates

768 are in fact possible because evaporation is not happening from a wide pool of liquid ethanol, but
769 instead from four different point sources, namely the tips of the four corner films. This means that
770 there is not only a vapor concentration gradient in the vertical direction but in all directions around
771 these point sources leading to much higher drying rates. We present these calculations here.

772 Firstly we can determine the potential evaporation from a free surface covered by ethanol. The
773 diffusive flux J_G across the atmospheric boundary layer of thickness δ equals the mass ΔM
774 transported through cross section ΔA per time interval Δt and is defined by Fick's law:

775 $$J_G = \frac{\Delta M}{\Delta A \Delta t} = -D\frac{\Delta c}{\delta} \quad (24)$$

776 with diffusion coefficient D and an ethanol concentration difference in the gas phase Δc (the
777 negative sign defines an upwards directed gas flow for decreasing concentration in upwards
778 direction). The diffusive flux of ethanol can be expressed as evaporation rate e_0 with density of liquid
779 ethanol ρ and volume ΔV as:

780 $$e_0 = \frac{\Delta V}{\Delta A \Delta t} = -\frac{D}{\rho}\frac{\Delta c}{\delta} \quad (25)$$

781 The mass of ethanol in the gas phase is defined by saturated vapor pressure p_s at the surface and
782 equals 0 at the top of the boundary layer. For a small gas volume V_U, the mass of ethanol M_U
783 within this vapor saturated volume can be deduced from the universal gas law:

784 $$p_s V_U = \frac{M_U}{M_M} RT \rightarrow M_U = \frac{p_s V_U M_M}{RT} \quad (26)$$

785 with molar Mass M_M, gas constant R, and temperature T. The concentration gradient across the
786 boundary layer (where ethanol vapor concentration is zero) can be expressed as function of M_U and
787 V_U and inserted in equation 25:

788 $$e_0 = -\frac{D}{\rho}\frac{p_s M_M}{RT}\frac{1}{\delta} \quad (27)$$

For high air velocities the thickness of the boundary layer is expected to be very thin, especially due to short lateral distances along the capillary that limit the evolution of thick boundary layers. For boundary layer thicknesses ranging between 0.1 and 1.0 mm, a density of liquid ethanol ρ of 789 kg m^{-3}, vapor pressure for ethanol of p_s =8000 Pa, temperature of 298 ˚K, molar mass M_M of 0.0461 kg/Mol, and diffusion coefficient of ethanol in air D of 1.1 10^{-5} m^2 s^{-1} the evaporation rate ranges between 1800 and 180 mm/day.

In addition, it must be taken into account that in the experiments ethanol is not evaporating from a large pool of liquid but from a small capillary of size d within a large volume of surrounding atmosphere. To apply the concept of Schlünder [24] to estimate evaporation from a liquid filled patch within an area of size L with boundary layer, we firstly express the square shape capillary size d by a circular structure of radius r with identical cross-section:

$$\pi r^2 = d^2 \rightarrow r = \frac{d}{\sqrt{\pi}} \tag{28}$$

According to Schlünder [24], the evaporation rate from a square of size L with a wet element of size r equals:

$$e = e_0 \frac{1}{1 + \frac{2}{\pi}\frac{r}{\delta}\sqrt{\frac{\pi}{4\phi}}\left(\sqrt{\frac{\pi}{4\phi}} - 1\right)} \tag{29}$$

with evaporation rate from free ethanol surface e_0, and the cross-sectional fraction of wet patch ϕ that can be expressed by L and d. The evaporation rate e assigned to the total area L^2 origins from evaporation from the wet area d^2, with evaporation rate e_p related to the water-filled cross-section (after a few calculation steps):

$$e_p = e_0 \frac{2\pi\delta L^2}{d\left(-2d\,L + L^2\sqrt{\pi} + 2d\,\delta\pi\right)} \tag{30}$$

For a relatively low drying rate of 180 mm/day and a boundary layer thickness of 1 mm, the evaporation rate per pore e_p reaches a maximum for $L = 2\delta\pi$ of 700 mm/day. To summarize:

While extreme evaporation rates above 1000 mm/day are caused by thin boundary layers for high air flow velocities, rates of a few hundreds mm per day are supported by large spacings and formation of a spherical vapor shell around the capillary.

5.5 link to real porous media

The square capillary model provides a tool to study the basic physical mechanics that limit the duration of stage 1 and limit the extent of a capillary sustained film region in which flow can occur. Similar drying dynamics will be observed in all kinds of angular capillary geometries since capillarity in such geometries leads to the presence of thick corner films leading to advection dominated stage 1. This type of films is an important constituent of the film region in real porous media since pores are in general angular shaped instead of perfectly circular. However the extent of the corner films in a single angular capillary cannot directly lead to quantitative conclusions of film region extent in real porous media. The maximum extent of the corner films in our experiments is in the end highly dependent on capillary geometry. A different capillary cross section, for example triangular, would influence this maximum film length L_c, but also the rounded corners showed to have a large effect on film length. Thus to use this model to simulate drying from a real medium as a bundle of different angular fibers requires a lot of detailed knowledge on medium structure of pore sizes and pore geometry. A future aim could be to upscale these results and define a certain average angularity of the pores in the medium as well as a pore size distribution and tortuosity which affects the direction of the gravity component in each section of the film.

A simple application of the model could be to represent the entire film region with the square capillary, by choosing capillary size and corner radius r_0 in an appropriate way. The capillary size defined by width d determines at which suction the capillary becomes air invaded, and thus would need to be fitted to the air entry value of the macroscale medium. r_0 defines the suction at which the film region would retreat from the surface if only gravity force opposing capillary force is considered. This suction could for example be the air entry value of the smallest pores at the surface of the

porous medium. In this way the range of suction values at which there are corner films in the single capillary represents the whole pore size distribution of the real porous medium.

6. Summary and Conclusion

Evaporation of the two liquids ethanol and water was studied from a single glass capillary with square cross section. Such a capillary geometry shows the same drying stages as drying from real porous media with an advection dominated stage 1 where drying rates are high, followed by diffusion dominated stage 2 with constantly dropping drying rates. The break-up of corner films that are present in the capillary corners determines the transition between these two stages. This is reflected in high drying rates before break-up, followed by a significant drop during the break-up of the films. The corner films provide the pathways between main meniscus and capillary surface through which the liquid can flow. Similar dynamics can be observed in drying from real porous media, where a capillary sustained film region can provide the interconnected liquid pathways for advectional transport. Corner films in the square capillary provide an analogue for this film region, while the main meniscus can be compared to the retreating drying front in real porous media.

A modeling approach was developed to predict a characteristic maximum extent of liquid corner films L_C that develop in angular capillaries during the process of liquid evaporation. L_C was determined by a balance between capillary force retaining the liquid in the corners, opposed by gravity and viscous losses. Reducing the gravity component that opposes the capillary force by orienting the capillary in smaller angles with the horizontal plane leads to larger values for L_C. Viscous losses only come into play as soon as flow occurs through the films leading to smaller L_C values for increased evaporation rates due to higher flow resistances.

Experiments on ethanol evaporation showed that the model is predicting L_C values pretty well. Underlying simplifying assumptions of the model are a constant drying flux before film break-up and

phase change of liquid to vapor only taking place at the tips of the films. In the experiments it turned out to be that drying rates already start dropping slightly before film break-up. Limitations from coupling between capillary surface and atmospheric boundary layer is a possible explanation. Dye deposition patterns show that diffusion/ phase changes are taking place along the corner film interface up to a certain depth inside the capillary of maximum twice the capillary width. These observations show that the model assumptions are indeed simplifying the actual drying process but the agreement between experimental and modeling results show that this is not affecting L_C predictions significantly.

Experiments with water show that the nonzero contact angle leads to more irregular behavior as opposed to ethanol evaporation. Film break-up of different corners had a large variation and usually occurred somewhere halfway the film. Also there was no trend in experimental results with increased evaporation rates. A possible explanation is that the films in this case have a smaller suction range over which they can exist, which makes them already break up due to mechanical limitations before viscous losses become very significant. This makes them also highly sensitive to small variations in corner radii and explains why they seem to be unaffected by different evaporation rates.

To use the corner flow model for representing a porous medium as a bundle of angular capillaries requires detailed knowledge of pore geometries and sizes. However a simple application could be to represent drying from a real porous medium by choosing capillary width d and corner radius r_0 wisely such that the suction range over which the films exist represents all pore sizes and their air entry values.

Summary of units and values of different parameters

Property	**Symbol**	**Unit**
Capillary width	d	m
Gravitational acceleration	g	9.81 m/s^2
Drainage snap-off radius	r_d	m
Capillary corner radius	r_0	m
Critical head value	h_d	m
Head value at which r= r_0	h_{min}	m
Roundedness	Ro	-
Capillary corner half angle	α	π/2
Initial evaporation rate	e_0	m/s
Cross-sectional area of the capillary	A^{tot}	m^2
Radius of curvature coefficient	C_{nd}	-
Angularity factor	F_n	-

885

7. Acknowledgements

This research was conducted at the Soil and Terrestrial Environmental Physics (STEP) group at ETH Zürich, Switserland. I would like to thank prof. Dani Or and dr. Peter Lehmann from the STEP group for their great supervision on my masters research. Their critical guidance and good ideas have made me get the best out of my seven months stay at the ETH. I got a lot of opportunities to form a clear view on academic research including the chance to go to the European General Union Assembly 2012 in Vienna with a poster presentation. Also the techniciens of the STEP laboratory, Hans Wünderli and Daniel Breitenstein, were of great help when I was having all the sorts of problems that can come up when performing experiments.

I would also like to thank prof. ir. Majid Hassanizadeh for his guidance throughout my master in Environmental Hydrogeology at the University of Utrecht. His broad academic network and interest in his students has brought me this opportunity to conduct my research abroad.

8. References

[1] P. Lehmann, S. Assouline and D. Or, *Phys. Rev. E,* **77**, 056309, (2008).

[2] G. W. Scherer, *J. Am. Ceram. Soc.,* **73**, 3, (1990).

[3] J. Van Brakel, in *Advances in Drying*, New York, Hemisphere, (1980), p. 217.

[4] S. Suzuki and S. Maeda, *J. Chem. Eng. Jpn.,* **1**, 26, (1968).

[5] N. Shokri, P. Lehmann and D. Or, *Water Resour. Res.,* **45**, W10433, (2009).

[6] A. G. Yiotis, A. K. Stubos, A. G. Boudouvis and I. N. Y. Y. C. Tsimpanogiannis, *Transp. Porous Media,* **58**, 63, (2005).

[7] A. G. Yiotis, A. G. Boudouvis, A. K. Stubos, I. N. Tsimpanogiannis und Y. C. Yortsos, *Phys. Rev. E,* **68,** 037303, (2003).

[8] M. Tuller and D. Or, *Water Resour. Res.,* **37**, 1257, (2001).

[9] A. G. Yiotis, A. K. Stubos, A. G. Boudouvis and Y. C. Yortsos, *Adv. Water Resour.,* **24**, 439, (2001).

[10] J. B. Laurindo and M. Prat, *Chem. Eng. Sci.,* **53**, 2257, (1997).

[11] M. Prat, *Int. J. Heat Mass Transfer,* **50**, 1455, (2007).

[12] F. Chauvet, P. Duru, S. Geoffroy and M. Prat, *Phys. Rev. Lett.,* **103**, 124502, (2009).

[13] G. Mason and N. R. Morrow, *J. Colloid Interface Sci.,* **141**, 1, (1991).

[14] M. Tuller, D. Or and M. Dudley, *Water Resour. Res.,* **35**, 7, (1999).

[15] D. Or and M. Tuller, *Water Resour. Res.,* **35**, 3591, (1999).

[16] M. Dong and I. Chatzis, *J. Colloid Interface Sci.,* **172**, 278, (1995).

[17] F. Chauvet, P. Duru and M. Prat, *Phys. Fluids,* **22**, 112113, (2010).

[18] T. C. Ransohoff and C. J. Radke, *J. Colloid Interface Sci.,* **121**, 392, (1987).

[19] Y. Chen and M. M. N. C. L. Weislogel, *J. Fluid Mech. ,* **566**, 235, (2006).

[20] D. Zhou, M. Blunt and F. M. Orr, *J. Colloid Interface Sci.,* **187**, 11, (1996).

[21] G. Mason and N. R. Morrow, *J. Colloid Interface Sci.,* **141**, 262, (1991).

[22] J. Bico and D. Quéré, *J. Colloid Interface Sci.,* **247**, 162, (2002).

[23] W. Brutsaert and D. Chen, *Water Resour. Res.,* **31**, 1305, (1995).

[24] E. U. Schlünder, *Chem. Eng. sci.,* **43**, 2685, (1988).

900

901

902